Atmos. Meas. Tech. Discuss., https://doi.org/10.5194/amt-2019-135
Manuscript under review for journal Atmos. Meas. Tech.
Discussion started: 23 April 2019


Atmospheric Measurement Techniques
Discussions

# Analysis of the lightning production of convective cells

Jordi Figueras i Ventura[1], Nicolau Pineda[2,3], Nikola Besic[1], Jacopo Grazioli[1], Alessandro Hering[1], Oscar A. van der Velde[3], David Romero[3], Antonio Sunjerga[4], Amirhossein Mostajabi[4], Mohammad Azadifar[5], Marcos Rubinstein[5], Joan Montanyà[3], Urs Germann[1], and Farhad Rachidi-Haeri[4]

[1]MeteoSwiss, Locarno, Switzerland
[2]Meteorological Service of Catalonia, Barcelona, Spain
[3]Universitat Politècnica de Catalunya UPC, Terrassa, Spain
[4]École Polytechnique Fédérale de Lausanne EPFL, Lausanne, Switzerland
[5]Haute Ecole Spécialisée de Suisse occidentale HES-SO, Yverdon-les-bains, Switzerland

**Correspondence:** Jordi Figueras i Ventura (jordi.figuerasiventura@meteoswiss.ch)

**Abstract.** This paper presents an analysis of the lightning production of convective cells. The cells were detected by the MeteoSwiss Thunderstorms Radar Tracking (TRT) algorithm in the course of a lightning measurement campaign that took place in the summer of 2017 in the area surrounding the Säntis mountain, in the northeastern part of Switzerland. For this campaign, and for the first time in the Alps, a Lightning Mapping Array (LMA) was deployed. In the first part of the paper, we examine the relationship between the intra-cloud (IC) and cloud-to-ground (CG) activity and the cell severity as derived by the TRT algorithm of a large dataset of cells gathered during the campaign. We also propose and analyze the performance of a new metric to quantify lightning intensity, the rimed particles column (RPC) height and base altitude. In the second part, we focus on two of the most severe cells detected during the campaign that produced significantly different outcomes in terms of the lightning activity. The paper shows that the newly proposed metric (RPC) seems to be a very promising predictor of lightning activity, particularly for IC flashes. Future lightning nowcasting algorithms in any case should be probabilistic in nature and incorporate the polarimetric properties of the convective cells as well as the lightning climatology.

## 1 Introduction

Current meteorological warnings are strictly based on meteorological features. However there is a societal need for more impact-based meteorological warnings (WMO Public Weather Services Programme, 2015). Impact-based warnings would allow more effective preventive actions and an optimization of the deployment of the emergency services in the most critical areas. In order to issue impact-based warnings though, the type of natural hazard has to be identified and forecasted with precision since the required preventive and response actions to be taken for each meteorological phenomenon may be different. Lightning activity nowcasting systems are still lacking lacking in precision and reliability. Warnings on lightning activity would be very valuable in many areas such as the organization of outdoors events, for the safety in areas of high lightning risk (e.g.

Atmos. Meas. Tech. Discuss., https://doi.org/10.5194/amt-2019-135
Manuscript under review for journal Atmos. Meas. Tech.
Discussion started: 23 April 2019


warnings for maintenance personnel in wind farms or tall structures), airport warning systems, etc. Moreover, lightning jumps (Schultz et al., 2009) have been associated to severe weather intensification and therefore if lightning activity can be reliably nowcasted it can have a positive impact in the forecasting of other phenomena.

Since 2004, the Thunderstorms Radar Tracking (TRT) algorithm is operational at MeteoSwiss (Hering et al., 2004). This algorithm identifies, tracks and characterizes convective cells in real-time with 5-min resolution using data from the operational C-band polarimetric weather radar network. The TRT algorithm ranks the identified cells in 5 categories according to their severity. The position of each cell is extrapolated 60 minutes into the future according to its moving direction and speed. That is part of the semi-automatized short-term severe weather warnings issued by MeteoSwiss (Hering et al., 2015). The level of the warning is based on the cell rank category: weak (for which no warning is issued), developing, moderate, severe and very severe. Implicit in such categories there is information of expected precipitation intensity, wind gusts and hail. Explicit lightning activity warnings are output by a separate system but they are issued only for airports. The lightning warning is relatively simple and consists primarily on the observation of the lightning activity in the area surrounding the airports. Clearly an explicit forecast of the lightning activity within the context of convective cells would be an appreciated enhancement.

Lightning activity can be roughly divided into intra- or inter-cloud (IC) and cloud-to-ground (CG) categories. CG flashes can be reliably detected and located using continental-scale networks of low frequency sensors such as the EUCLID network in Europe. Such networks, though, are not as efficient at detecting IC flashes (Poelman et al., 2016). Lightning mapping arrays (LMAs), on the other hand, provide 3D information of the discharge path with a much higher temporal and spatial resolution. An LMA is a network of VHF sensors that measure the arrival time of VHF radiation and uses the information to estimate the location of the intracloud channel sources (Proctor, 1971). The return stroke in CG strokes does not produce such intense VHF emissions as lightning leaders and therefore it is not evident to classify flashes as CG. Hence, both types of networks are complementary.

In this paper we analyze a large number of convective cells detected during a lightning measurement campaign that took place in the summer of 2017 in the area surrounding the Säntis mountain, northeast of Switzerland. For this campaign, and for the first time in the Alps, an LMA was deployed. The main goals of this study are:

- To explore the relationship between the TRT cell rank and the lightning activity (both intra-cloud IC and cloud-to-ground CG).

- To present and evaluate the performance of a new indicator of possible lightning activity based on polarimetric radar data, the rimed particles column (RPC) base altitude and height.

- To examine in detail and compare the characteristics of two convective cells that reached similar levels of severity but produced very different outputs in terms of lightning activity.

The paper is organized as follows: Section 2 provides a brief overview of the Säntis measurement campaign and the instrumentation and methods used for this study. Section 3 contains a statistical analysis of the entire dataset. Section 4 presents a detailed analysis of two severe convective cells. General conclusions and recommendations are given in section 5.

## 2 Instrumentation and methods

The Säntis measurement campaign was a joint venture between the Electromagnetic Compatibility Laboratory (EMC LAB) of the Swiss Federal Institute of Technology in Lausanne (EPFL), the Institute for Information and Communication Technologies of the University of Applied Sicences of Western Switzerland (HES-SO), the Lightning Research Group (LRG) of the Technical University of Catalonia, the Meteorological Service of Catalonia (meteo.cat) and the Radar Satellite and Nowcasting Division of the Federal Office of Meteorology and Climatology MeteoSwiss. The campaign took place in the summer of 2017. The main objective of the campaign was to study the atmospheric conditions leading to lightning production in the vicinity of the Säntis telecommunications tower, with particular focus on the upward lightning discharges initiated by the tower itself. In this study, though, we focus on the lightning production of convective cells regardless of their origin. The 124 m tall telecommunications tower is situated on top of the Säntis mountain (47.2429°N, 9.3393°E, 2502 m MSL), in the Sankt Gallen Canton, in the north-eastern part of Switzerland. The main instruments of the campaign were in-situ measurements on the tower, including lightning current and static electric field measurements, a Lightning Mapping Array (LMA) network and a polarimetric Doppler weather radar network. The area covered by the campaign and the location of the instrumentation can be seen in Fig. 1. In the following, a brief description of the instrumentation used during the campaign is provided.

### 2.1 Radar data

#### 2.1.1 The operational MeteoSwiss Doppler polarimetric weather radar network

MeteoSwiss owns and operates a network of 5 C-band, Doppler polarimetric weather radars. The network was recently renewed within the project Rad4Alp, which was concluded in 2016 (Germann et al., 2015). The 5 systems have identical specifications and modes of operation. The scanning strategy consists of 20 horizontal scans with elevations ranging from -0.2° to 40° repeated every 5 min. The elevations are inter-leaved: every 2.5 min a half-volume of 10 elevations from top to bottom is concluded. A very short pulse of 0.5 µs is used to obtain data with a range resolution of 83.3 m with angular resolution of 1°. IQ data are processed on-site using standard techniques (e.g., Doviak and Zrnic, 2006) to obtain the basic polarimetric moments, i.e., reflectivity (horizontal $Z_h$ and vertical $Z_v$), differential reflectivity ($Z_{dr}$), co-polar correlation coefficient ($\rho_{hv}$) and raw co-polar differential phase ($\psi_{dp}$) as well as Doppler moments. These basic moments are transmitted to a central server. The operational data processing involves a clutter detection using a sophisticated decision tree filter (DT-filter) and a reduction of the resolution to 500 m by averaging 6 consecutive gates (only clutter-free ones). From the low resolution polarimetric moments all subsequent products are generated. For the measurement campaign, data from the Albis radar (47.2843°N 8.5120°E, 938 m MSL), situated 63 km east of the Säntis tower were used (see Fig. 1).

#### 2.1.2 The Thunderstorms Radar Tracking (TRT) algorithm

Since 2004 MeteoSwiss operates the automatic Thunderstorms Radar Tracking algorithm TRT (Hering et al., 2004). The algorithm identifies, tracks and characterizes convective cells in real-time with 5 minutes resolution using as input the reflectivity data from the 3D radar composite (1 km horizontal resolution and 200 m vertical resolution up to 18 km MSL) and the iso-0°C from NWP models and lightning data from the EUCLID network as auxiliary parameters. The detection of the cells is based on a dynamic thresholding scheme applied on the reflectivity data of multiple-radar composites. For each radar pixel, the columnar maximum reflectivity is defined. A cell is defined as a connected area of radar pixels larger than a given area threshold and whose reflectivity exceeds an adaptive detection threshold. The detection threshold is chosen so that 1) it is above a minimum, 2) the difference between the max value of the cell and a member pixel is above a certain threshold, 3) the area covered by the cell is smaller than a certain threshold. The cells are currently classified in five categories (weak [0-1.2[, developing [1.2-1.5[, moderate [1.5-2.5[, severe[2.5-3.5[ and very severe [3.5-4.0[) according to their severity ranking (Hering et al., 2008). The categorization is performed by examining the values of vertical integrated liquid content (VIL [$\mathrm{kg \cdot m^{-2}}$]), median cell echo top 45 dBZ ($ET45m$ [km]), maximum cell reflectivity ($dBZmax$ [dBZ]) and the extension of the area of the cell having a reflectivity above 55 dBZ ($area55dBZ$ [$\mathrm{km^2}$]):

$$RANK = (2 \cdot VIL + 2 \cdot ET45m + dBZmax + 2 \cdot area55dBZ)/7.0 \quad (1)$$

The tracking of the cell is performed by searching areas of overlap between cells of two consecutive images (the current time $t$ and the previous one $t$-$t_0$). The cells at $t$-$t_0$ are advected using the estimated cell velocity and the overlapping area between the advected cell and each of the cells detected at time $t$ is computed. Cells with the maximum overlapping area, provided that it is above a minimum threshold, are considered to be the same and given the same unique ID. The velocity of each cell is computed by examining the displacement of the cell center between two consecutive images and taking the weighted average of all previous velocities, calculated recursively with a decreasing weight, or by a cross-correlation technique if no displacement of the cell centres can be found. Once the cell has been properly identified, various parameters are computed to better characterize the cell. The parameters computed are summarized in Table 1. All these parameters are stored in a file (one file per radar image every 5 minutes). This information, accessible also in real-time, is very useful to study the evolution of the convective cells.

#### 2.1.3 Additional radar data processing and analysis tools

A specific non-operational processing was performed on radar data obtained in real time during the campaign. The processing was performed using the Python-based open source software Pyrad/Py-ART (Figueras i Ventura et al., 2017). Detailed information on the processing is provided in Figueras i Ventura et al. (2019). It is sufficient to mention here that at the end of the processing, high resolution (83.3 m) clutter-free volumes of attenuation-corrected horizontal reflectivity $Z_h$ and differential refletivity $Z_{dr}$, co-polar correlation coefficient $\rho_{hv}$, specific differential phase $K_{dp}$, air temperature from the Numerical Weather Prediction (NWP) model COSMO-1 (see http://www.cosmo-model.org/) re-sampled at the radar resolution and the dominant hydrometeor type at each range gate were obtained. The hydrometeor classification is described in Besic et al. (2016) and it provides the following hydrometeor classes: aggregates (AG), ice crystals (CR), light rain (LR), rimed particles (RP), rain (RN), vertically-oriented ice crystals (VI), wet snow (WS), melting hail (MH), ice hail-high density graupel (IH) and no classification (No valid radar data) NC. These data were used in the subsequent analysis.

Within the radar data processing tool Pyrad, a TRT trajectory function has been implemented. This function uses the cell footprints defined by the TRT algorithm to extract all the (3D) radar volume data contained within its boundaries. The 3D volume corresponds to the vertical extrapolation of the 2D cell footprint of the TRT, i.e. its section is invariant with height. Out of this dataset, several products can be generated. For example, one product computes histograms over the entire vertical data column, another computes various quantiles, a 3rd product obtains a profile of user-defined statistics (mean, median, mode, etc.) at prescribed height levels, etc. A similar rationale is used also to extract data obtained by the LMA within the TRT cell footprint.

Out of the hydrometeor-classification cell profile constructed by taking the mode at each height level of 250 $\mathrm{m}$ resolution we compute the RPC height as the difference between the maximum and minimum altitudes where rimed particles or hail are predominant. The possibility that height levels within this column have other predominant hydrometeors is neglected since we assume that isolated rimed particle areas cannot exist so in any case a significant if not dominant proportion of hydrometeors would be rimed particles.

### 2.2 Ligthning mesurements

Lightning detection was performed using two networks, the European Cooperation for Lightning Detection Network (EUCLID) Schulz et al. (2016) and an LMA network specifically deployed for the campaign. Both networks are described in more detail in Figueras i Ventura et al. (2019). It is sufficient to mention here that the EUCLID network has a high CG flash detection efficiency (on the order of 95%), but a reduced IC detection efficiency. The EUCLID network provides information of the location of the lightning strokes, intensity and polarity. The LMA network consisted of 6 VHF sensors which were provided by LRG. The LMA sensors detect VHF sources generated by lightning leaders and provides 3D information of the source location (including the altitude). A post-processing algorithm clusters together individual sources deemed to be part of the same flash and assigns them a unique ID number. Since the detection of the lightning leaders requires direct line of sight of the source, LMAs observe with high efficiency intra-cloud (IC) activity, mostly from negative leaders moving through regions of positive charge. However, weaker sources from positive leaders moving through negative charge regions are often detected (van der Velde and Montanyà, 2013). In complex orography, cloud-to-ground (CG) activity is often detected indirectly from stepped negative leaders or, less often, from negative dart leaders and some times positive leaders as well.

## 3 General data analysis

The LMA was installed in the Säntis area between 29 June and 15 August 2017. In half of the days that the campaign lasted (24 out of 48) some lightning activity was registered in the LMA-covered area by the EUCLID network. Of these, on 15 days lightning activity was registered within 2 km from the Säntis tower. Within the 15 days of interest, there were a total of 257 cells crossing the reduced LMA domain visible in Fig. 1. On 8 of those 15 days LMA data were available. 22, 24 and 25 of July were excluded because less than 5 LMA stations were operational. Days 5, 8, 9 and 15 August were excluded also because, although enough stations were operating, for reasons still under investigation the data quality was poor.

The large majority of cells in the analysis (211) had a maximum severity rank of weak, 23 reached a rank corresponding to developing, 15 moderate and 8 severe. None were classified as very severe. The maximum rank achieved by a cell was 3.4. In 178 cells no EUCLID CG strokes were detected. Those cells were for the most part classified as weak or developing. Only one cell reached moderate status (2.1). The number of cells during days where LMA data were analyzed was 147. Out of these, 54 cells had lightning activity according to the LMA.

Most cells were traveling from west/south-west to east/north-east. The most severe cells originated outside of the reduced LMA domain and were crossing it already at a fairly mature state. The cells that spent their entire lifetime within the LMA domain boundaries tended to be shorter-lived and weaker. The highest rank of a cell generated and dissipating within the domain was moderate (2.1). As it can be seen in Fig. 2, there is a low correlation between the number of flashes detected within a TRT cell by the LMA network and those CG detected by the EUCLID network.

We are interested in determining whether any meaningful relationship can be established between radar data signatures and lightning activity. We will analyze radar data with respect to two metrics for lightning activity: the absolute number of flashes/sources within the cell domain and the density of flashes/sources considering the cell area. This second metric is used in order to account for the varying dimensions of a TRT cell due to the dynamic thresholding scheme. Fig. 3 shows a scatter plot of the TRT cell rank versus the number of CG strokes detected by the EUCLID network (left panel) and the CG stroke density (right panel). The figures show that there is a very weak correlation between cell ranking and lightning activity. The situation is slightly better when confronting rank versus LMA flashes (Fig. 4) or LMA sources (Fig. 5). In such case, although a significant number of points with high rank have few lightning activity, there seems to be an incremental increase in the number of flashes starting from rank 1. When considering only the reduced domain, some of the high rank points with no lightning activity disappear. Perhaps a bit counter-intuitively, the absolute number of flashes/sources seems to provide better correlation. This is due to the small size of the weak to moderate TRT cells. The number of flashes has better correlation with the cell rank than the number of sources.

We examine now the time of occurrence of the first maximum of lightning activity with respect to the time of occurrence of the first maximum rank within the TRT cell (see Fig. 6). Of the 257 cells for which EUCLID data are available, only in 79 were there flashes detected within the cell. In 22% of those cells the first maximum of strokes within the cell (19% when stroke density is considered) occurred before the maximum rank of the cell was achieved, 13% (13% as well) occurred simultaneously and 66% (68%) occurred after the maximum rank was achieved.

Of the 147 cells where LMA data was available, only 54 cells exhibited some lightning activity. Of these, in 19% of the cases the first maximum of flashes within the cell occurred before the first maximum rank was achieved (17% if flash density is used), in 24% of the cases it occurred simultaneously (28% for flash density) and 57% occurred after the first maximum rank (56% for flash density). If we consider only cells that move strictly within the LMA domain (not shown), there are 84 of these but, since in general they are short-lived and weak, only 19 of them produced lightning activity. However the ratio is approximately the same with 16% getting a maximum of flashes before the maximum rank, 37% simultaneously and 47% after. In fact, examining the cell rank when the first maximum of lightning activity is achieved (Fig. 7), it can be observed that in general it is not particularly high, suggesting that the peaks in lightning activity occur either at the development phase of the convective cell or once the cell is mature.

The prevalence of peaks of lightning activity well after the maximum cell rank is achieved is in line with past studies that have shown that very severe cells tend to have a reduced lightning activity right before and during their mature phase (e.g., Montanyà et al., 2007). The hypothesis for that is that the strong updraft characteristic of severe cells would lift the charge centers higher up (thus making it less likely for flashes to reach the ground) and prevent particles to grow and acquire charge at a given level (thus reducing the IC flashes likelihood).

From the data analysis in Figueras i Ventura et al. (2019) we inferred that most lightning activity was produced in areas where rimed particles or hail were predominant. Fig. 8 shows a scatter plot of RPC height versus flashes for both the EUCLID network CG strokes and the LMA network flash origins. Only data from the reduced LMA domain and during the days the LMA was active are considered . For the LMA detected flashes in particular (bottom panels), the correlation is rather high. Noticeable lightning activity starts roughly at a column height of 2000 $\mathrm{m}$ and largely increases with increasing height. Cloud to ground activity may occur even with modest heights but a long column (over 8000 $\mathrm{m}$) is a strong indicator of intense lightning activity. We have divided the data for CG activity (top panels) into CG+ (blue crosses), CG- (red crosses) and total lightning (green dots). Again there is a marked increase in lightning activity with RPC height, particularly above 8000 $\mathrm{m}$. It is worth noticing that when the RPC reaches such height and important proportion of the lightning activity is due to CG+ strokes. Moreover, when no RPC was retrieved, i.e. RPC height equals 0, The dominant type of stroke has positive polarity. If we examine the CG activity as a function of RPC base altitude (Fig. 9), it can be observed that there is a weak dependency. Indeed, lightning activity is low when the column starts above 5000 $\mathrm{m\,MSL}$, although it must be noticed the large peak in activity when the RPC base is located at 4500 $\mathrm{m\,MSL}$. It should be noticed that in such case a significant percentage is constituted by CG+ strokes. From this analysis it can be inferred that RPC length is a better indicator of lightning that RPC base altitude although perhaps a more adequate metric would be height with respect to the average or maximum ground altitude within the TRT cell.

## 4 Case study: Comparison of two severe TRT cells with different lightning efficiency

We analyze in more detail here two of the most severe cells encountered during the campaign. The first one occurred on day 2017-07-19 (TRT cell ID 2017071915100055 hereby cell 1) and reached a maximum rank of 3.1 while the second occurred on day 2017-08-01 (TRT cell ID 2017080116050003 hereby cell 2) and reached a maximum rank of 3.4. Both are therefore classified as severe. However, they diverge significantly in the number of CG strokes produced. While the first cell produced a peak of 16 CG strokes (stroke density of 0.035 $\mathrm{flashes \cdot km^{-2}}$), the second one reached 130 strokes (stroke density of 0.48 $\mathrm{flashes \cdot km^{-2}}$).

Fig. 10 shows graphs of the position, velocity and area of the two cells. The duration of the cells was similar (cell 1 2$\mathrm{h}$, cell 2 2.5$\mathrm{h}$) and they were first detected at similar times (Cell 1 at 15:10 UTC, cell 2 at 16:05). Cell 1 started south, close to the Alps, and moved somewhat erratically from south-west to north-east following the footsteps of the Alps. Initially it moved very fast towards north but it rapidly lost speed. Cell 2 moved rather fast on a narrow strip from west to east. Cell 1 started with a small area of less than 100 $\mathrm{km}^2$ and progressively grew up to more than 400 $\mathrm{km}^2$, then it likely split at 16:10 and merged again with another cell at 16:35, thereby reaching the maximum area. Cell 2 started with an already large area of more than 200 $\mathrm{km}^2$, progressively grew up to 600 $\mathrm{km}^2$ and at 17:35 it split into two and kept an area of roughly 200 $\mathrm{km}^2$.

In terms of ranking (see Fig. 11 top panels), cell 1 started as weak (ranking 0) but it reached moderate status rather fast (15 min) and stayed in that category for most of its lifespan except for two time steps ranked as severe in the first half of its life, at 15:50 and 15:55. Cell 2, on the other hand, was already developing when first detected but it took it 35 min to reach moderate status. It reached the category of severe at two time steps during the second part of its life, at 17:20 and 17:25. Cell 1 had very low CG lightning activity during the first part of its life (see Fig. 11 middle panels). The few lightning strokes produced during this period had all positive polarity except for one. At 16:10 there was a first peak in lightning activity and during the last part of its life it remained modestly active. The maximum activity was achieved at 16:40, although at this point the cell was relatively large so the stroke density was quite modest. For the most part of its lifetime there was a higher percentage of CG+ than CG-. Interestingly, there were no CG strokes detected during its peak ranking. Cell 2 had plenty of CG lightning activity during its entire lifespan. The peak maximum of 120 CG strokes was reached early on and well before the maximum rank was reached. In fact, at that time the cell rank was a modest 1.1. During the first part of its life, up to 16:50, there were very few CG+ strokes detected. After 16:50 there was another increase in ligthning activity but this time a significant proportion of strokes had positive polarity. The lightning activity remained rather high virtually till the end of the cell, with a significant proportion of CG+ strokes although that was never as dominant as with cell 1.

Unfortunately the cells only crossed the domain of maximum LMA detection for part of their life span (see Fig. 11 lower panels). However, this coincided with peaks of activity in the cell (towards the end of its life for cell 1 and midlife for cell 2). Significant differences can already be seen in the number of LMA flashes detected within the cell with respect to the number of CG strokes. Whereas cell 1 had a significant number of flashes detected (between 100 and 200) producing very modest CG activity (a maximum of 16 flashes), cell 2 had an even higher LMA flash detection (between 250 and 350) and a large number of flashes reached the ground (well above 60). Looking at the altitude where those LMA flashes were originated and propagated (Fig. 12), it can be seen that in the area with good LMA detection, most of the flashes originated within a narrow band between roughly 7000 and 9000 m MSL for cell 1 whereas those of cell 2 were more widespread but higher concentrations can be found higher up in the atmosphere, towards 9000 m MSL. When looking at the position of all VHF sources it is even more clear that sources of cell 2 propagated preferably at a lower altitude.

The main differences between the two cells though, can be observed in their vertical profiles (see Fig. 13, Fig. 14 and Fig. 15). Cell 1 had an RPC base altitude of roughly 4000 m MSL for its entire lifespan. Initially the RPC height was about 4000 m and progressively grew (with some fluctuations) up to 7000 m on average, coinciding with the time of maximum CG flash activity . Cell 2 on the other hand had an RPC base altitude slightly higher, around 4500 m MSL for most of its lifespan. What is noticeable is that the RPC height was much higher than that of cell 1. From the beginning of its life was on the order of 8000 m and reached a length in excess of 10000 m in the second part of its life, where it had also significant proportions of hail in it. Notice that after the cell split and due to the reduced size of the resultant cell, there were height levels where few radar data was available, hence the data gaps. The reflectivity values were also higher in general and with values higher than

30 dBZ well past 12000 m MSL suggesting the presence of larger and more abundant particles. $\rho_{hv}$ values above the freezing level were lower, particularly during the second part of its life, when large amounts of hail were present, a hint of a variety of particle shapes. It is also interesting to notice the large negative values of $K_{dp}$ during the second half of its life span, a feature that has been associated with lightning activity (Ryzhkov and Zrnic, 2007; Figueras i Ventura et al., 2013). In general, cell 2 exhibited large values of $K_{dp}$ below the freezing level. Cell 1 had also larger values of $K_{dp}$ below the freezing level when there was an increase in lightning activity but one should be cautious at interpreting that since the cell was moving very close to the Alps so it is likely that at those low altitudes the radar coverage was poor. Focusing on the frequency of occurrence of each value at each time stamp for cell 2 (see Fig. 16), it is worth noticing that when there was the first peak of lightning activity, there was a marked shift of the histogram of both $Z_{dr}$ and $K_{dp}$ towards positive values, a feature that may indicate the presence of $Z_{dr}$ columns, i.e. large updraft (Snyder et al., 2015).

## 5 Conclusions

In this paper we have presented an analysis of a large dataset of convective cells detected over the course of a lightning measurement campaign that took place in the summer of 2017 in the area surrounding the Säntis mountain, northeast Switzerland. In this campaign, for the first time in the Alps, a lightning mapping array was deployed. The use of the operational EUCLID network and the LMA network allows a thorough analysis of both the intra-cloud and the cloud-to-ground lightning activity within the convective cells.

The main conclusions of this study are:

- In general terms an increase in LMA flashes resulted in an increase of EUCLID flashes. However there were several outliers. In one case an excess of 500 LMA flashes resulted in few CG strokes and in another 30 CG strokes were detected without any apparent IC activity.

- Cells without lightning activity during their life cycle were mostly classified as weak but the rank of the convective cell is a poor indicator of its lightning activity, particularly considering CG flashes. In half of the cells studied the maximum of lightning activity was reached after the maximum rank was reached and in a quarter it was reached before. Generally speaking, the maximum ligthning activity was reached at the time period when cells were classified as weak to moderate.

- A more promising predictor of lightning activity seems to be the altitude of the rimed particles column, particularly for IC flashes. An increase in lightning activity was clearly shown from 3000 m onward. High CG lightning activity was observed when the rimed particle column was larger than 8000 m.

- The detailed study of two cells with similar characteristics but with different levels of CG lightning activity showed that there were significant differences in the composition of the solid phase region of the convective cloud. The cell with less lightning activity had a shallower RPC, a lower proportion of hail and in general lower reflectivity values and higher $\rho_{hv}$ values, suggesting smaller and more homogeneous particles.

This study has shown in the first place the usefulness of an LMA network even in a complex terrain such as the Swiss Alps in order to better characterize the intra-cloud lightning activity. It has also shown that a new parameter, rimed particles column, may be used within the context of cell severity warnings to add more explicit information of lightning activity. From this study it can be concluded that a radar-based lightning nowcasting system should be essentially probabilistic and take into account among others the rimed particle column height and position and the orography and man-made structures or alternatively the lightning climatology.

*Code and data availability.* Code used to post-process the radar data is available on github https://github.com/meteoswiss-mdr. Data is available on request by contacting the authors.

*Author contributions.* JFV performed the radar data processing and the data analysis contained in this paper. NB and JG contributed to the radar data processing and data interpretation. OvV, DR, JM, NP, AS, AM, MA, MR and FR deployed the LMA network and processed its data. UG 5 and AH advised on the content of the manuscript. JFV, with contributions from all authors, prepared the manuscript.

*Competing interests.* The authors declare that they have no conflict of interest.

*Acknowledgements.* This work was partially supported by the Swiss National Science Foundation (Project No. 200020_175594), the European Union's Horizon 2020 research and innovation program under grant agreement No 737033-LLR, research grants from the Spanish Ministry of Economy and the 421 European Regional Development Fund (FEDER): ESP2013-48032-C5-3-R, ESP2015-69909-C5-5-R422 and ESP2017-86263-C4-2-R.

## References

Besic, N., Figueras i Ventura, J., Grazioli, J., Gabella, M., Germann, U., and Berne, A.: Hydrometeor classification through statistical clustering of polarimetric radar measurements: a semi-supervised approach, Atmospheric Measurement Techniques, 9, 4425–4445, https://doi.org/10.5194/amt-9-4425-2016, https://www.atmos-meas-tech.net/9/4425/2016/, 2016.

Doviak, R. and Zrnic, D.: Doppler Radar and Weather Observations, Dover Books on Engineering Series, Dover Publications, https://books.google.ch/books?id=ispLkPX9n2UC, 2006.

Figueras i Ventura, J., Honoré, F., and Tabary, P.: X-Band Polarimetric Weather Radar Observations of a Hailstorm, Journal of Atmospheric and Oceanic Technology, 30, 2143–2151, https://doi.org/10.1175/JTECH-D-12-00243.1, https://doi.org/10.1175/JTECH-D-12-00243.1, 2013.

Figueras i Ventura, J., Leuenberger, A., Kuensch, Z., Grazioli, J., and Germann, U.: Pyrad: A Real-Time Weather Radar Data Processing Framework Based on Py-ART, in: 38th AMS Conference on Radar Meteorology, Chicago, IL, USA, 2017.

Figueras i Ventura, J., Pineda, N., Besic, N., Grazioli, J., Hering, A., van der Velde, O. A., Romero, D., Sunjerga, A., Mostajabi, A., Azadifar, M., Rubinstein, M., Montanyà, J., Germann, U., and Rachidi-Haeri, F.: Polarimetric radar characteristics of lightning initiation and propagating channels, Atmospheric Measurement Techniques Discussions, 2019, 1–45, https://doi.org/10.5194/amt-2019-31, https://www.atmos-meas-tech-discuss.net/amt-2019-31/, 2019.

Germann, U., Boscacci, M., Gabella, M., and Sartori, M.: Peak performance: Radar design for prediction in the Swiss Alps, Meteorological Technology International, 4, 42–45, 2015.

Hering, A., Morel, C., Galli, G., Sénési, S., Ambrosetti, P., and Boscacci, M.: Nowcasting thunderstorms in the Alpine region using a radar-based adaptive thresholding scheme, in: 3rd European Conference Radar in Meteorology and Hydrology (ERAD), Visby, Sweden, 2004.

Hering, A., Germann, U., Boscacci, M., and Sénési, S.: Operational nowcasting of thunderstorms in the Alps during MAP D-PHASE, in: 5th European Conference on Radar in Meteorology and Hydrology (ERAD), Helsinki, Finland, 2008.

Hering, A. M., Nisi, L., della Bruna, G., Gaia, M., Nerini, D., Ambrosetti, P., Hamann, U., Trefalt, S., and Germann, U.: Fully automated thunderstorm warnings and operational nowcasting at MeteoSwiss, in: 8th European Conference on Severe Storms ECSS 2015, Vienna, Austria, 2015.

Montanyà, J., Soula, S., and Pineda, N.: A study of the total lightning activity in two hailstorms, Journal of Geophysical Research: Atmospheres, 112, https://doi.org/10.1029/2006JD007203, https://agupubs.onlinelibrary.wiley.com/doi/abs/10.1029/2006JD007203, 2007.

Poelman, D. R., Schulz, W., Diendorfer, G., and Bernardi, M.: The European lightning location system EUCLID – Part 2: Observations, Natural Hazards and Earth System Sciences, 16, 607–616, https://doi.org/10.5194/nhess-16-607-2016, https://www.nat-hazards-earth-syst-sci.net/16/607/2016/, 2016.

Proctor, D. E.: A hyperbolic system for obtaining VHF radio pictures of lightning, Journal of Geophysical Research (1896-1977), 76, 1478–1489, https://doi.org/10.1029/JC076i006p01478, https://agupubs.onlinelibrary.wiley.com/doi/abs/10.1029/JC076i006p01478, 1971.

Ryzhkov, A. V. and Zrnic, D. S.: Depolarization in Ice Crystals and Its Effect on Radar Polarimetric Measurements, Journal of Atmospheric and Oceanic Technology, 24, 1256–1267, https://doi.org/10.1175/JTECH2034.1, https://doi.org/10.1175/JTECH2034.1, 2007.

Schultz, C. J., Petersen, W. A., and Carey, L. D.: Preliminary Development and Evaluation of Lightning Jump Algorithms for the Real-Time Detection of Severe Weather, Journal of Applied Meteorology and Climatology, 48, 2543–2563, https://doi.org/10.1175/2009JAMC2237.1, https://doi.org/10.1175/2009JAMC2237.1, 2009.

Schulz, W., Diendorfer, G., Pedeboy, S., and Poelman, D. R.: The European lightning location system EUCLID – Part 1: Performance analysis and validation, Natural Hazards and Earth System Sciences, 16, 595–605, https://doi.org/10.5194/nhess-16-595-2016, https://www.nat-hazards-earth-syst-sci.net/16/595/2016/, 2016.

Snyder, J. C., Ryzhkov, A. V., Kumjian, M. R., Khain, A. P., and Picca, J.: A ZDR Column Detection Algorithm to Examine Convective Storm Updrafts, Weather and Forecasting, 30, 1819–1844, https://doi.org/10.1175/WAF-D-15-0068.1, https://doi.org/10.1175/WAF-D-15-0068.1, 2015.

van der Velde, O. A. and Montanyà, J.: Asymmetries in bidirectional leader development of lightning flashes, Journal of Geophysical Research: Atmospheres, 118, 13,504–13,519, https://doi.org/10.1002/2013JD020257, https://agupubs.onlinelibrary.wiley.com/doi/abs/10.1002/2013JD020257, 2013.

WMO Public Weather Services Programme: WMO Guidelines on Multi-hazard Imapct-based Forecast and Warning Services, Tech. rep., World Meteorological Organization, 2015.

Atmos. Meas. Tech. Discuss., https://doi.org/10.5194/amt-2019-135
Manuscript under review for journal Atmos. Meas. Tech.
Discussion started: 23 April 2019


Atmospheric Measurement Techniques Discussions

**Table 1.** TRT cell parameters computed operationally

| **Parameter** | **Units** | **Definition** |
|---|---|---|
| $det$ | dBZ | Reflectivity cell detection threshold |
| $RANKr$ | – | $10 \cdot RANK$ of the cell |
| $ET45$, $ET45m$ | km MSL | Maximum/Median altitude of the 45 dBZ reflectivity echo |
| $ET15$, $ET15m$ | km MSL | Maximum/Median altitude of the 15 dBZ reflectivity echo |
| $VIL$ | $\mathrm{kg \cdot m^{-2}}$ | Vertically integrated liquid |
| $maxH$, $maxHm$ | km | Height of maximum reflectivity (of the echo with maximum reflectivity within the cell/median within the cell) |
| $CG-$, $CG+$, $CG$ | – | Number of negative/positive/total cloud to ground ligthning strikes within the cell (from EUCLID network) |
| $\%CG+$ | % | Percentage of positive cloud to ground lightning strikes within the cell respect to total (from EUCLID network) |
| $velx$, $vely$ | $\mathrm{km \cdot h^{-1}}$ | Estimated cell velocity on the x (east-west) axis/y (south-north) axis |
| $Dvelx$, $Dvely$ | $\mathrm{km \cdot h^{-1}}$ | Standard deviation of the current time step x-axis/y-axis cell velocity respect to the previous time step |
| $area$ | $\mathrm{km^2}$ | cell area |
| $cellcontourlon-lat$ | $^\circ$ | latitude-longitude of delimiting points of a polygon enclosing the cell |
| $lon$, $lat$ | $^\circ$ | longitude/latitude of the center of the cell |
| $ellL$, $ellS$ | km | Long/short axis of an ellipsis with equivalent area as the cell |
| $ellor$ | $^\circ$ | Orientation of an ellipsis with equivalent area as the cell |

**Table 2.** Analyzed days with some of their general characteristics. The LMA domain refers to the yellow area in Fig. 1. The cells considered have a life span of at least 3 radar time steps (i.e. 15 min) and have been present within the domain for at least 3 time steps

| Days examined | LMA | TRT cells within | TRT cells crossing | Max cell rank |
|---|---|---|---|---|
| 2017.06.29 | 6 | 14 | 8 | 1.4 |
| 2017.06.30 | 5 | 9 | 5 | 2.1 |
| 2017.07.10 | 5 | 12 | 13 | 1.4 |
| 2017.07.14 | 5 | 36 | 15 | 1.5 |
| 2017.07.18 | 5 | 7 | 5 | 2.6 |
| 2017.07.19 | 5 | 3 | 5 | 3.1 |
| 2017.07.22 | 4 | 1 | 6 | 2.7 |
| 2017.07.24 | 3 | 11 | 15 | 1.1 |
| 2017.07.25 | 3 | 21 | 17 | 1.3 |
| 2017.07.30 | 6 | 3 | 6 | 1.9 |
| 2017.08.01 | 6 | 0 | 6 | 3.4 |
| 2017.08.05 | 5 | 7 | 8 | 2.8 |
| 2017.08.08 | 5 | 5 | 4 | 0.5 |
| 2017.08.09 | 5 | 1 | 2 | 0.4 |
| 2017.08.15 | 5 | 9 | 3 | 1.8 |

Atmos. Meas. Tech. Discuss., https://doi.org/10.5194/amt-2019-135
Manuscript under review for journal Atmos. Meas. Tech.
Discussion started: 23 April 2019

Atmospheric Measurement Techniques
Discussions
Open Access

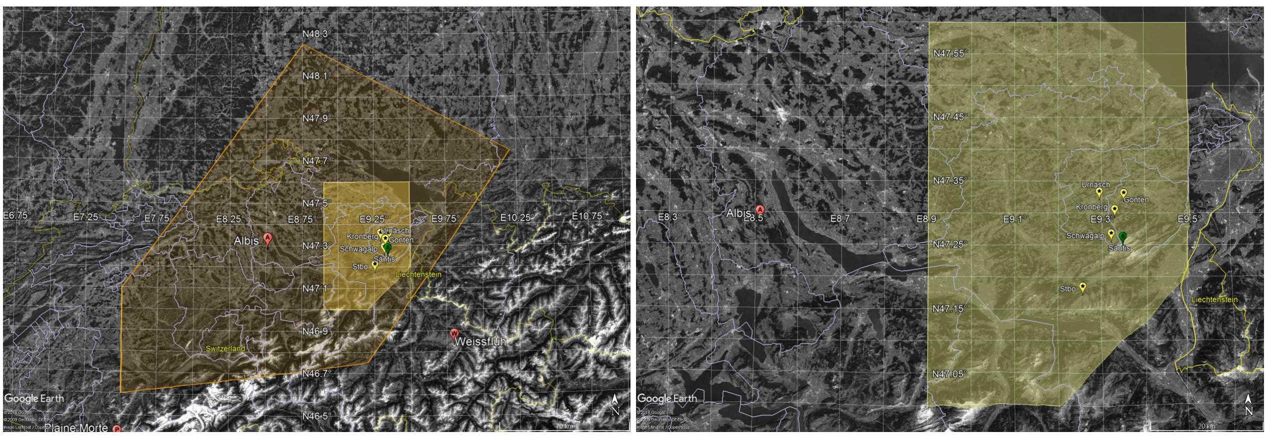


**Figure 1.** Left: Approximate extent of the maximum area covered by the LMA (Orange poligon). The yellow area shows the region with more comprehensive coverage. Radar positions are marked by red dots while the position of the LMA sensors is marked by yellow dots. The Säntis tower is marked by a green dot. Right: Zoom over the best covered area

Atmos. Meas. Tech. Discuss., https://doi.org/10.5194/amt-2019-135
Manuscript under review for journal Atmos. Meas. Tech.
Discussion started: 23 April 2019


Atmospheric Measurement Techniques Discussions

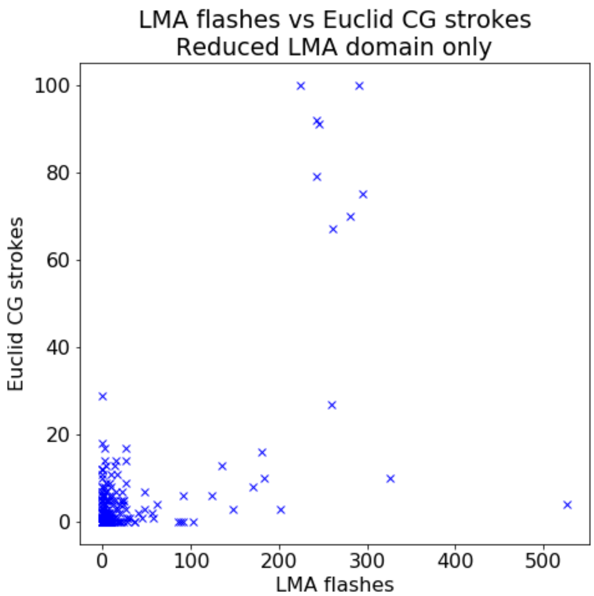


**Figure 2.** Scatter plot of number of flashes detected by the LMA network with respect to number of CG strokes detected by the EUCLID network in the reduced domain.

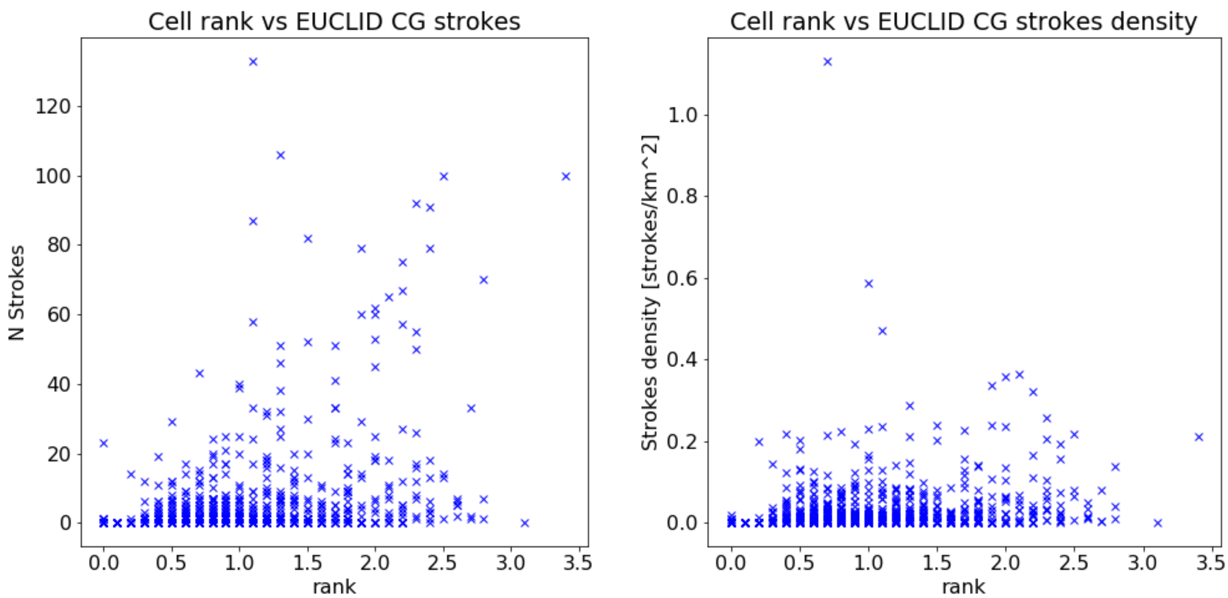


**Figure 3.** Scatter plot of rank versus: Left panel: Number of CG strokes within the TRT cell detected by the EUCLID network. Right panel: Density with respect to cell area. There are a total of 2792 points in the graph

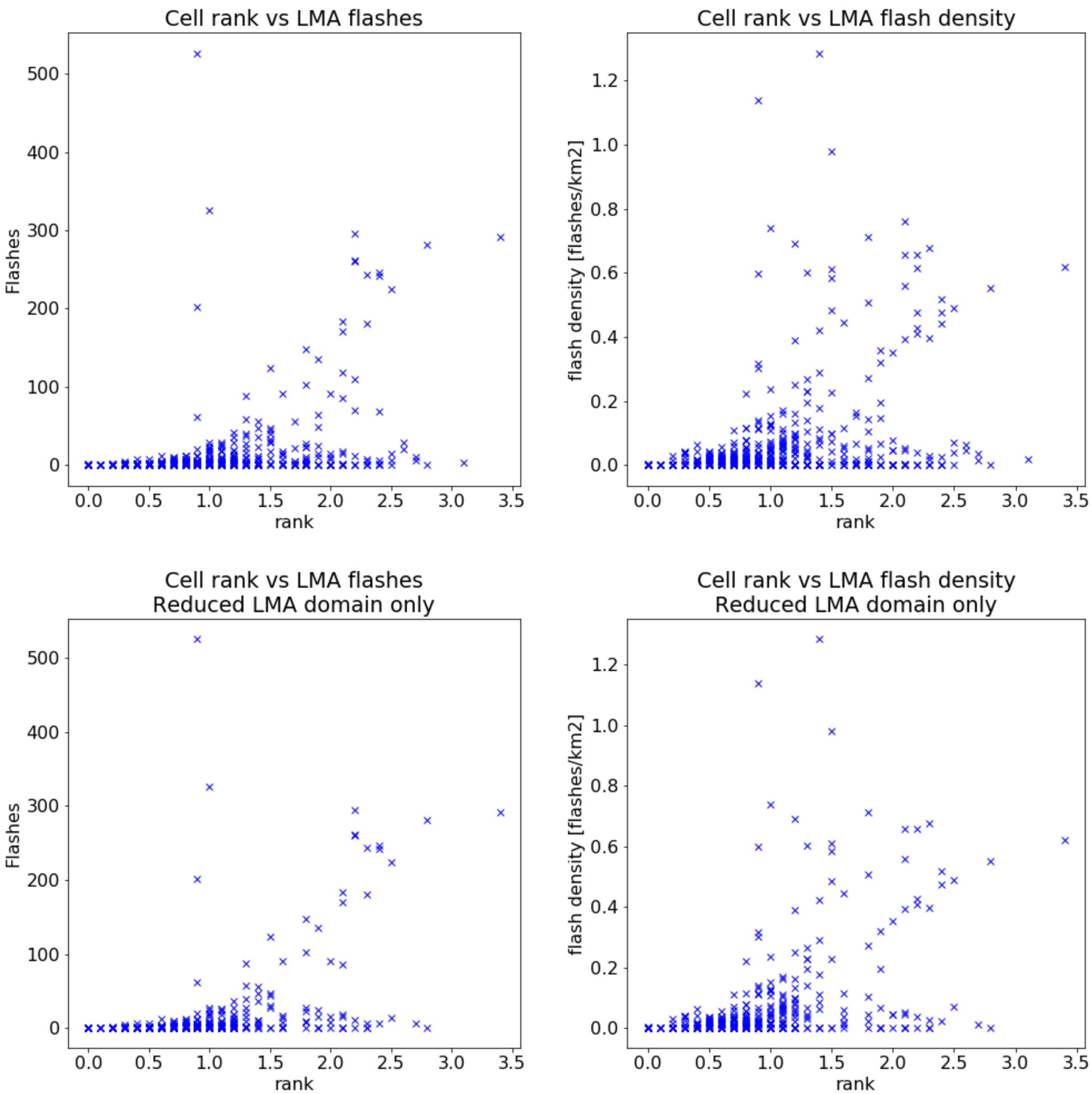


**Figure 4.** Scatter plot of rank versus: Left: Number of first VHF sources within the TRT cell detected by the LMA network. Right: Density with respect to cell area. Top: All detections, 1571 points. Bottom: Detections only when center of TRT cell within reduced domain, 965 points

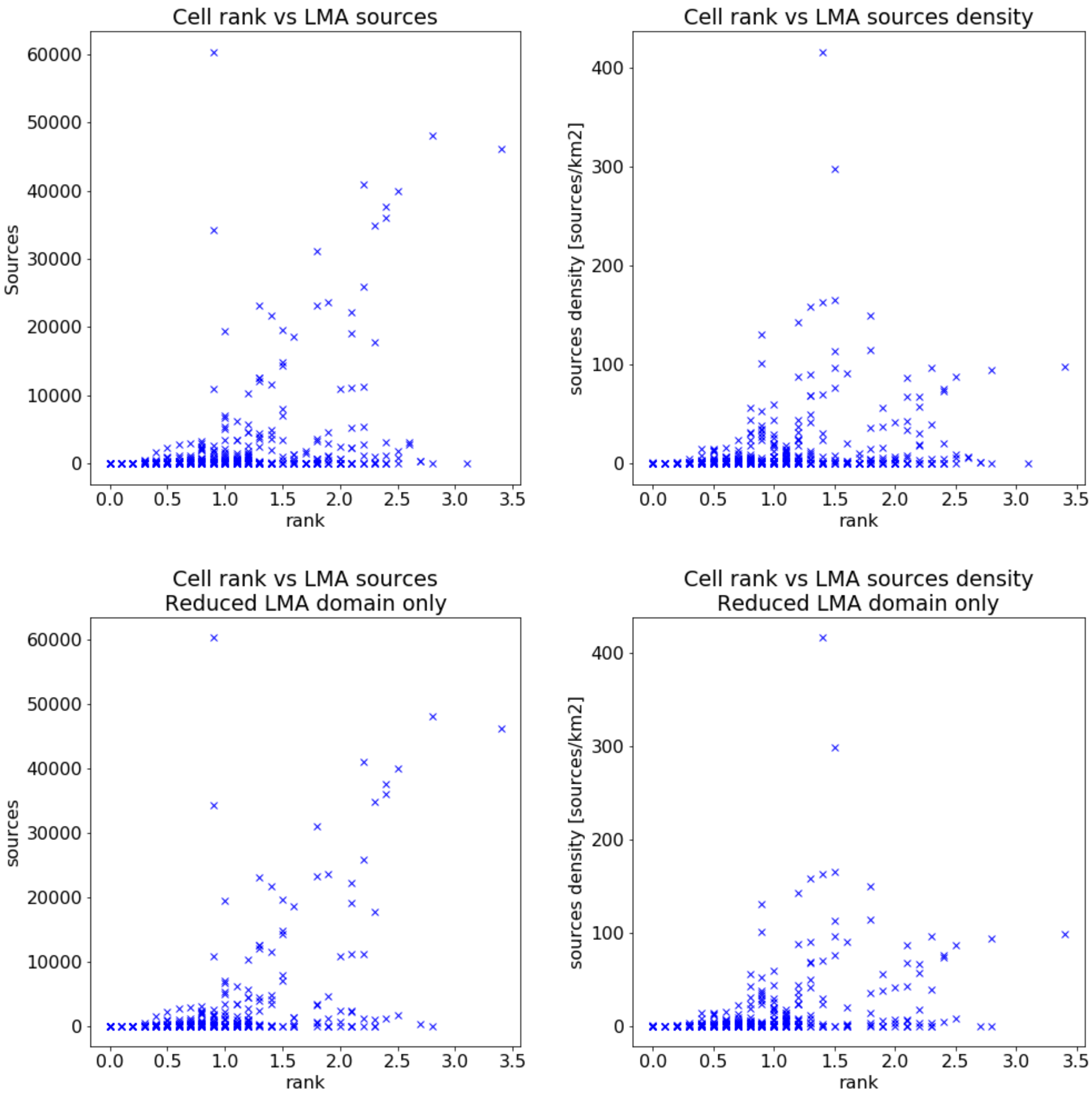


**Figure 5.** As in Fig. 4 but for LMA sources

Atmos. Meas. Tech. Discuss., https://doi.org/10.5194/amt-2019-135
Manuscript under review for journal Atmos. Meas. Tech.
Discussion started: 23 April 2019


Atmospheric Measurement Techniques
Discussions

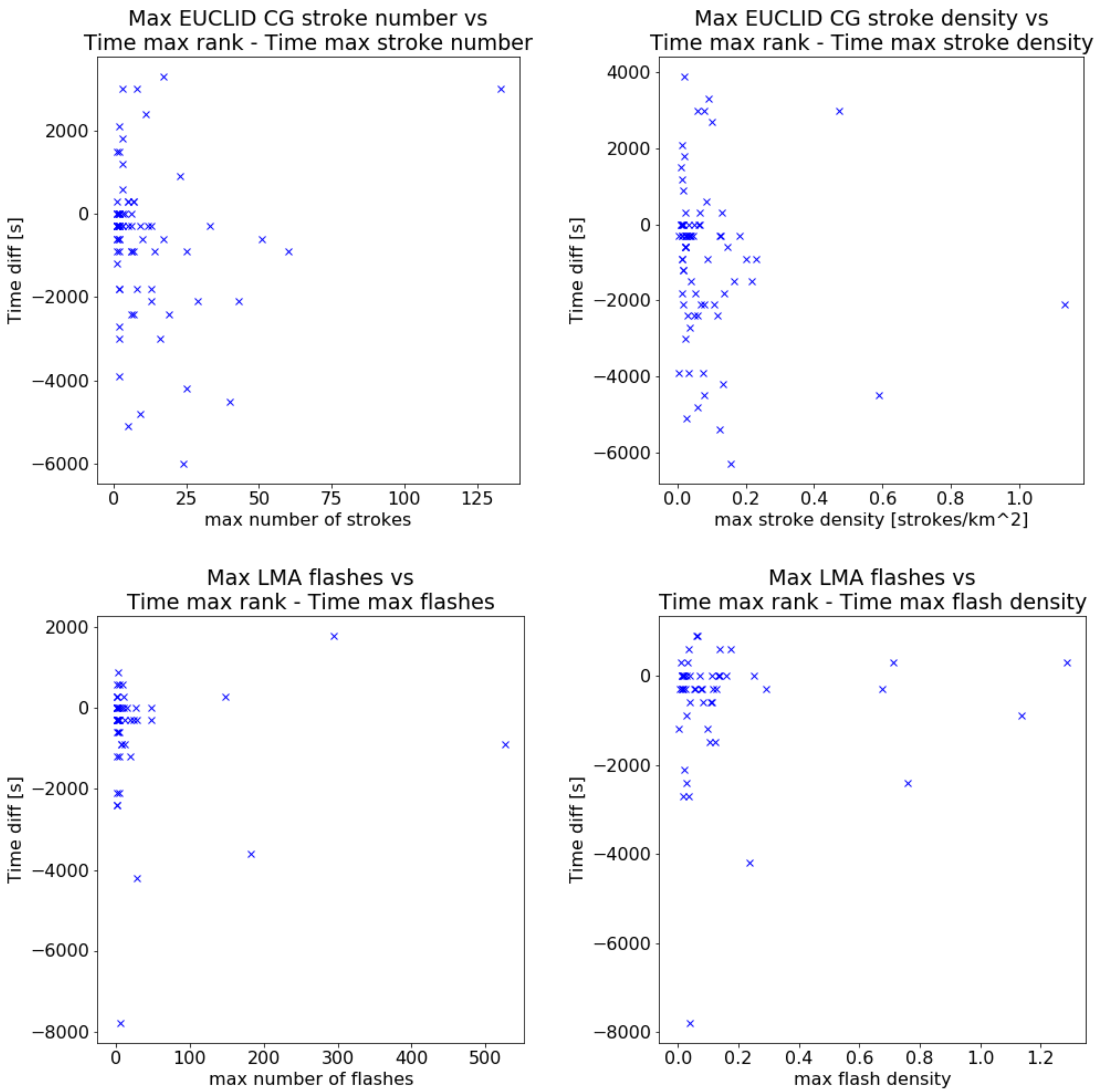


**Figure 6.** Scatter plot of: Top left: Max number of CG strokes detected by the EUCLID network with respect to time difference between occurrence of max rank and occurrence of max flashes, Top right: same as top left but for stroke density, Bottom left: Same as top left but for LMA detected flashes, Bottom right: Same as top right but for LMA detected flashes

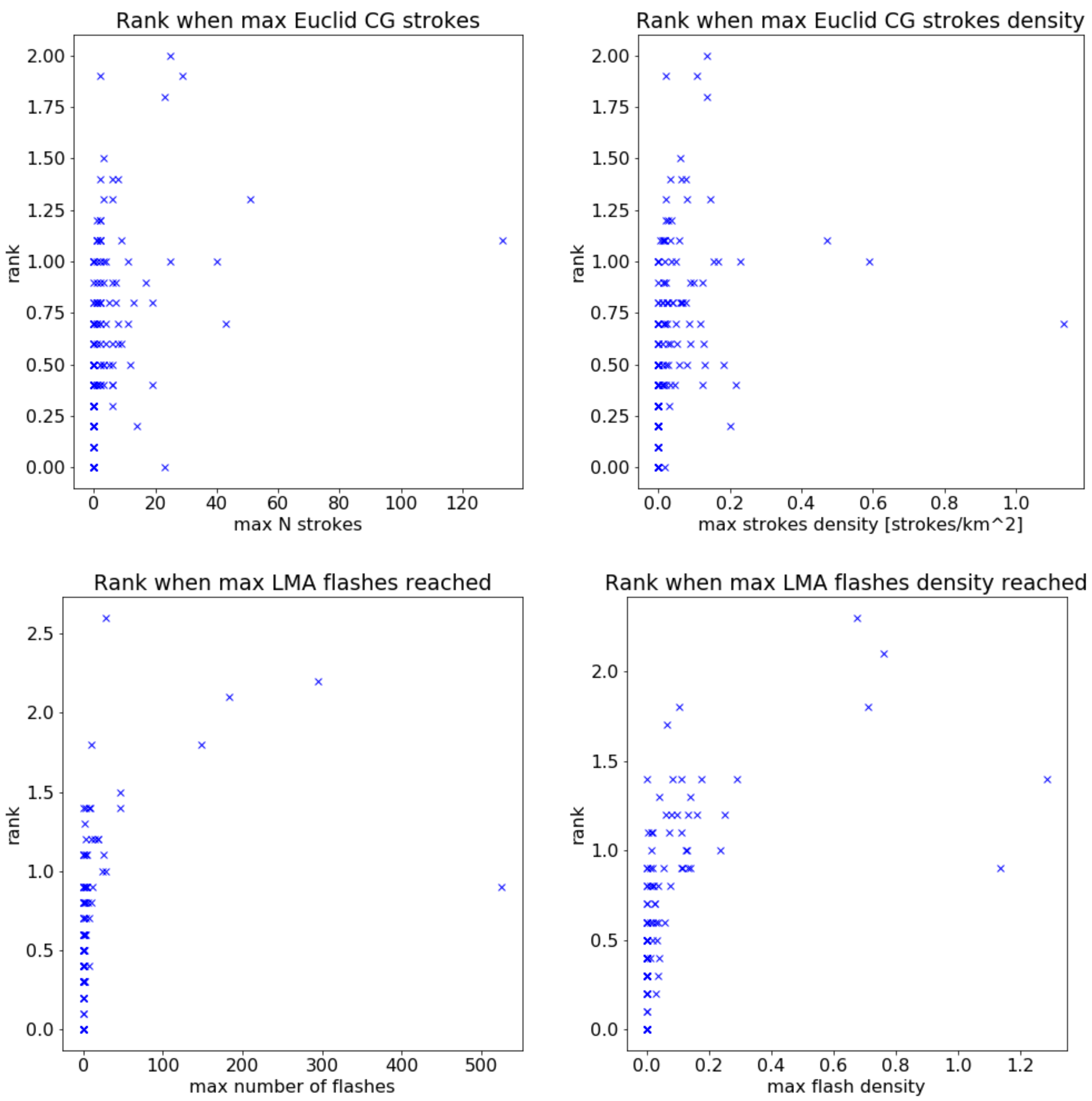


**Figure 7.** Scatter plot of: Top left: Cell rank when the first max number of CG strokes detected by the EUCLID network is achieved, Top right: same as top left but for stroke density, Bottom left: Same as top left but for LMA detected flashes, Bottom right: Same as top right but for LMA detected flashes

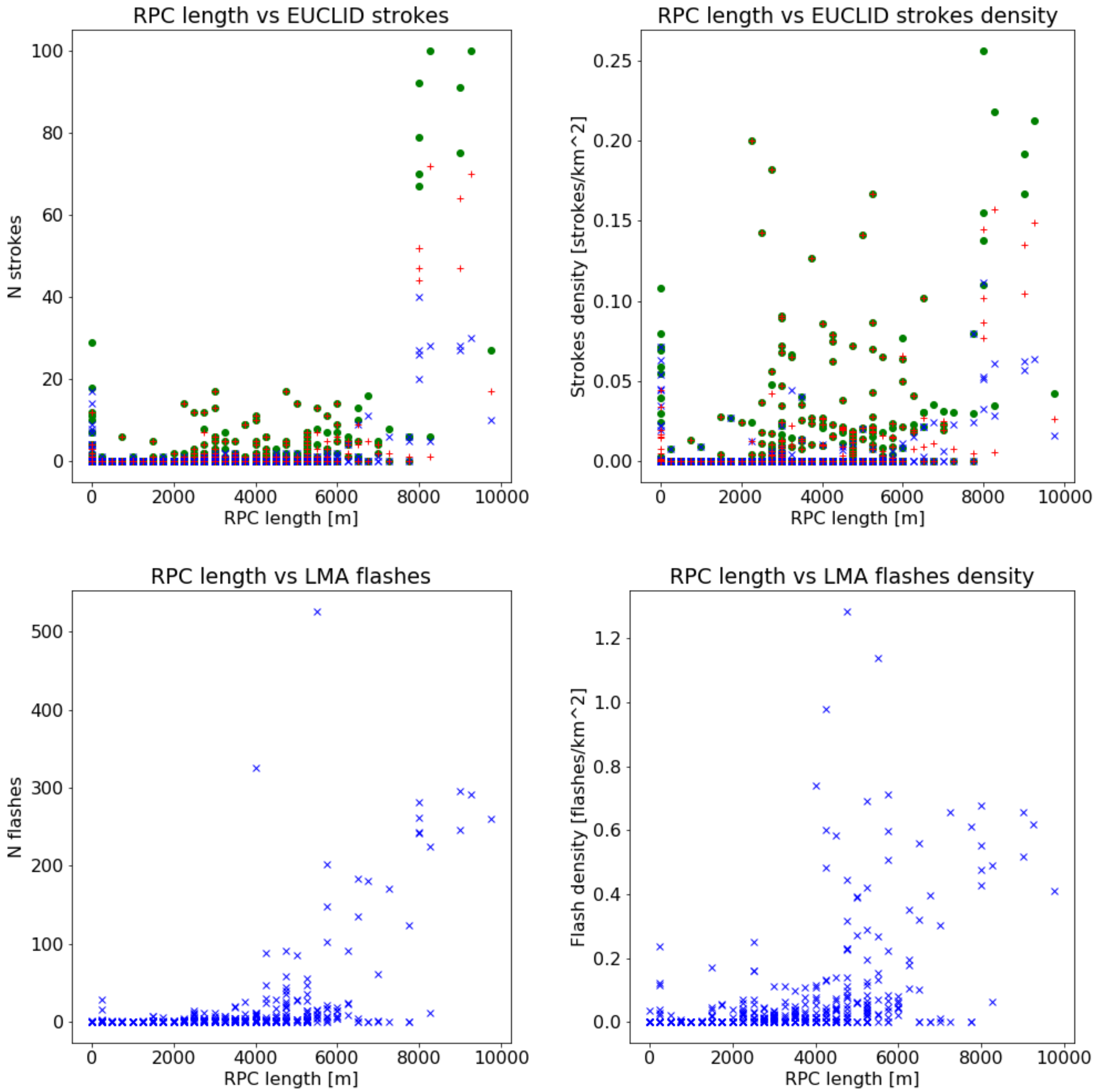


**Figure 8.** Scatter plot of RPC height versus: Left: Number of flashes within the TRT cell detected. Right: Density with respect to cell area. Top: EUCLID CG strokes. Blue crosses CG+ strokes, red crosses CG- strokes, green dots total lightning. Bottom: LMA first sources

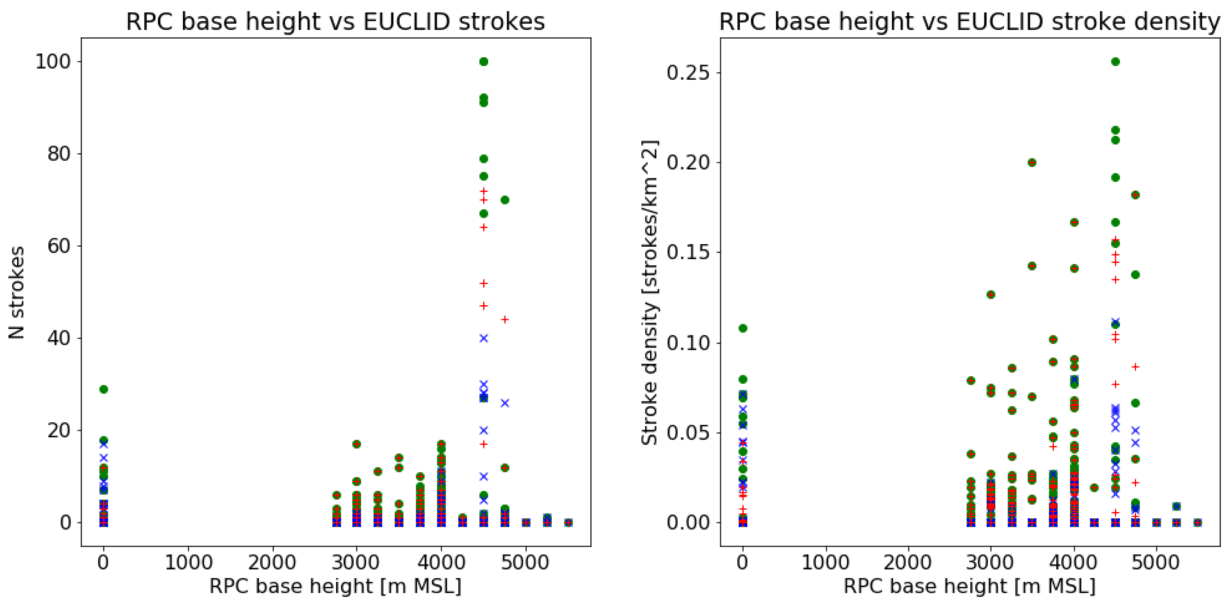


**Figure 9.** Scatter plot of RPC height versus: Left: Number of EUCLID CG strokes within the TRT cell detected. Right: Density with respect to cell area. Blue crosses CG+ strokes, red crosses CG- strokes, green dots total lightning

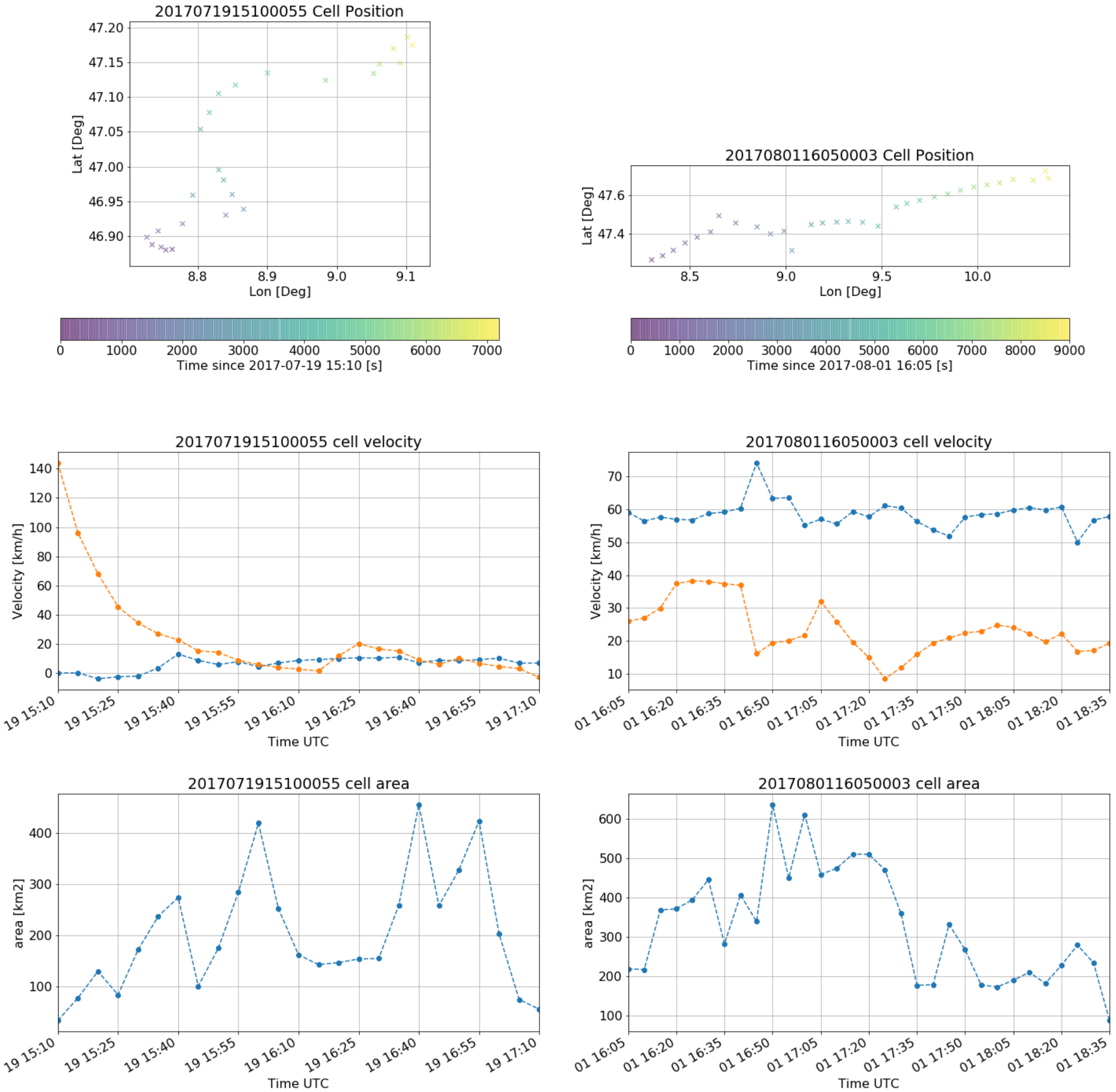


**Figure 10.** Top to bottom: Cell position, velocity (orange South-North direction, blue East-West direction) and area. Left: Cell 1, Right: Cell 2

Atmos. Meas. Tech. Discuss., https://doi.org/10.5194/amt-2019-135
Manuscript under review for journal Atmos. Meas. Tech.
Discussion started: 23 April 2019


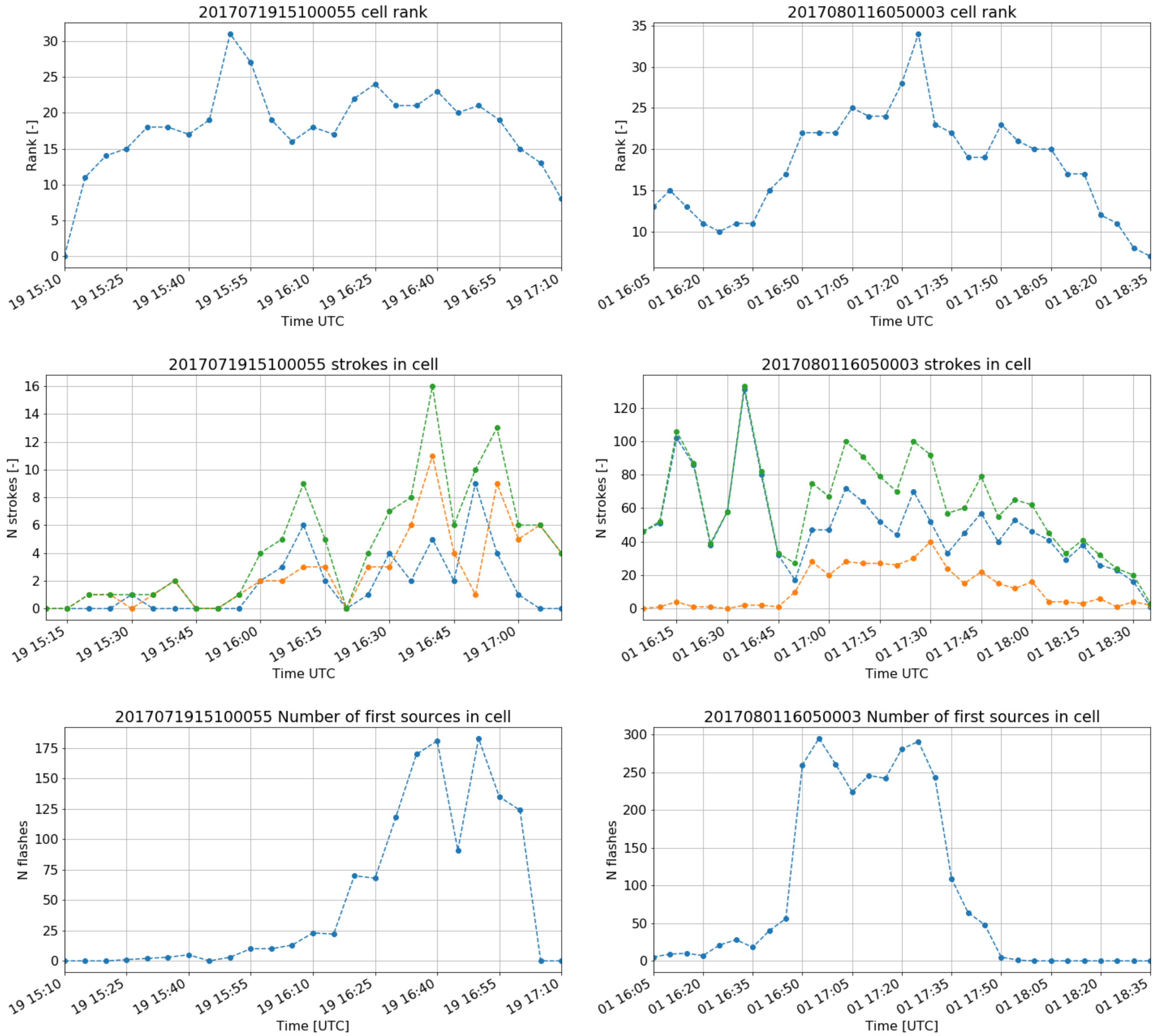


**Figure 11.** Top to bottom: 10xCell rank, EUCLID CG strokes (orange positive, blue negative, green total) and LMA detected flashes. Left: Cell 1, Right: Cell 2

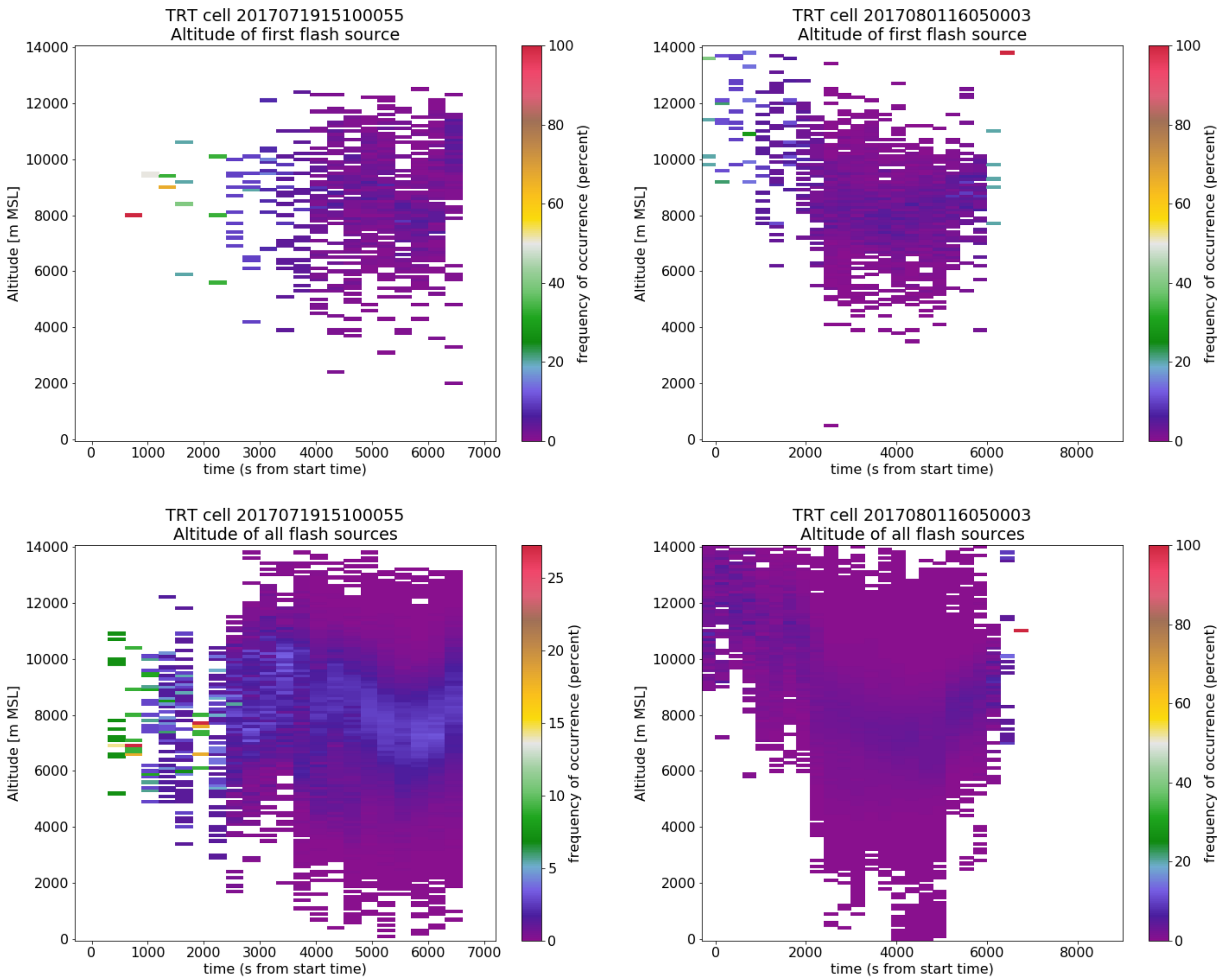


**Figure 12.** Top: Percentage of LMA flashes within the cell originated at each altitude, Bottom: Percentage of LMA flashes located at each altitude within the cell. Left: Cell 1, Right: Cell 2

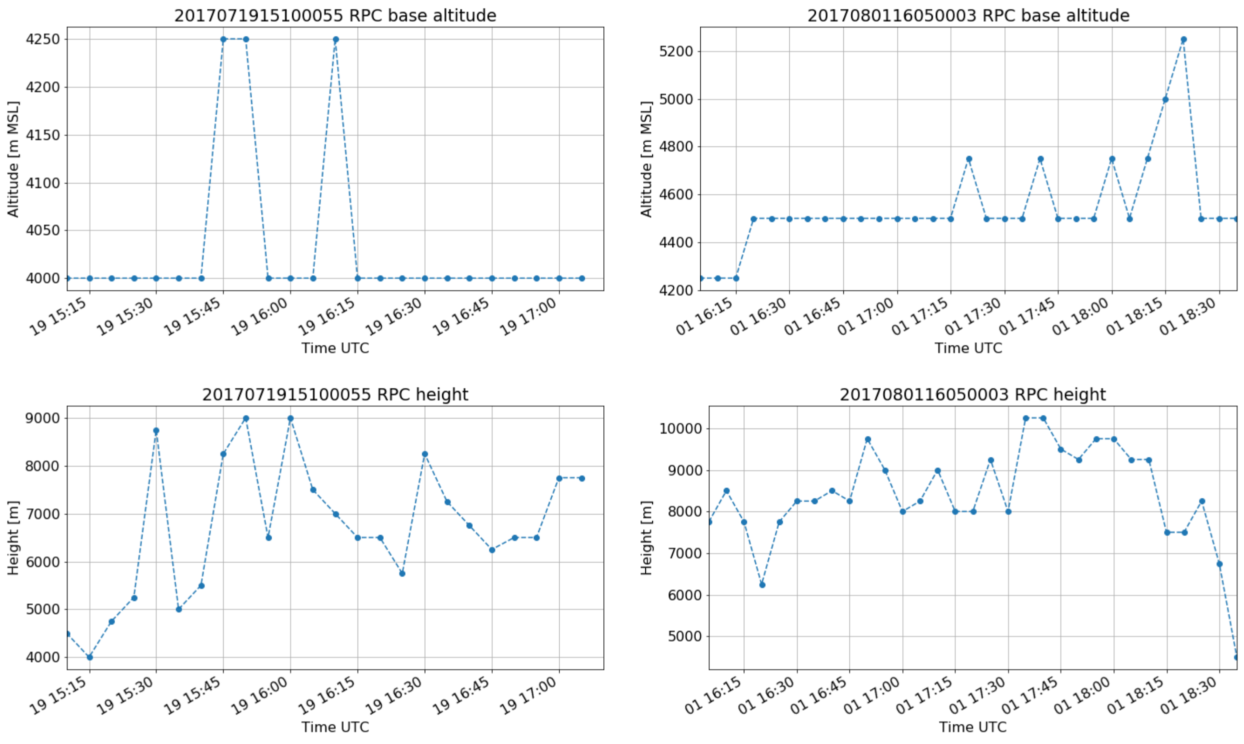


**Figure 13.** Top: RPC base altitude, Bottom: RPC height. Left: Cell 1, Right: Cell 2

Atmos. Meas. Tech. Discuss., https://doi.org/10.5194/amt-2019-135
Manuscript under review for journal Atmos. Meas. Tech.
Discussion started: 23 April 2019

Atmospheric Measurement Techniques
Open Access
Discussions

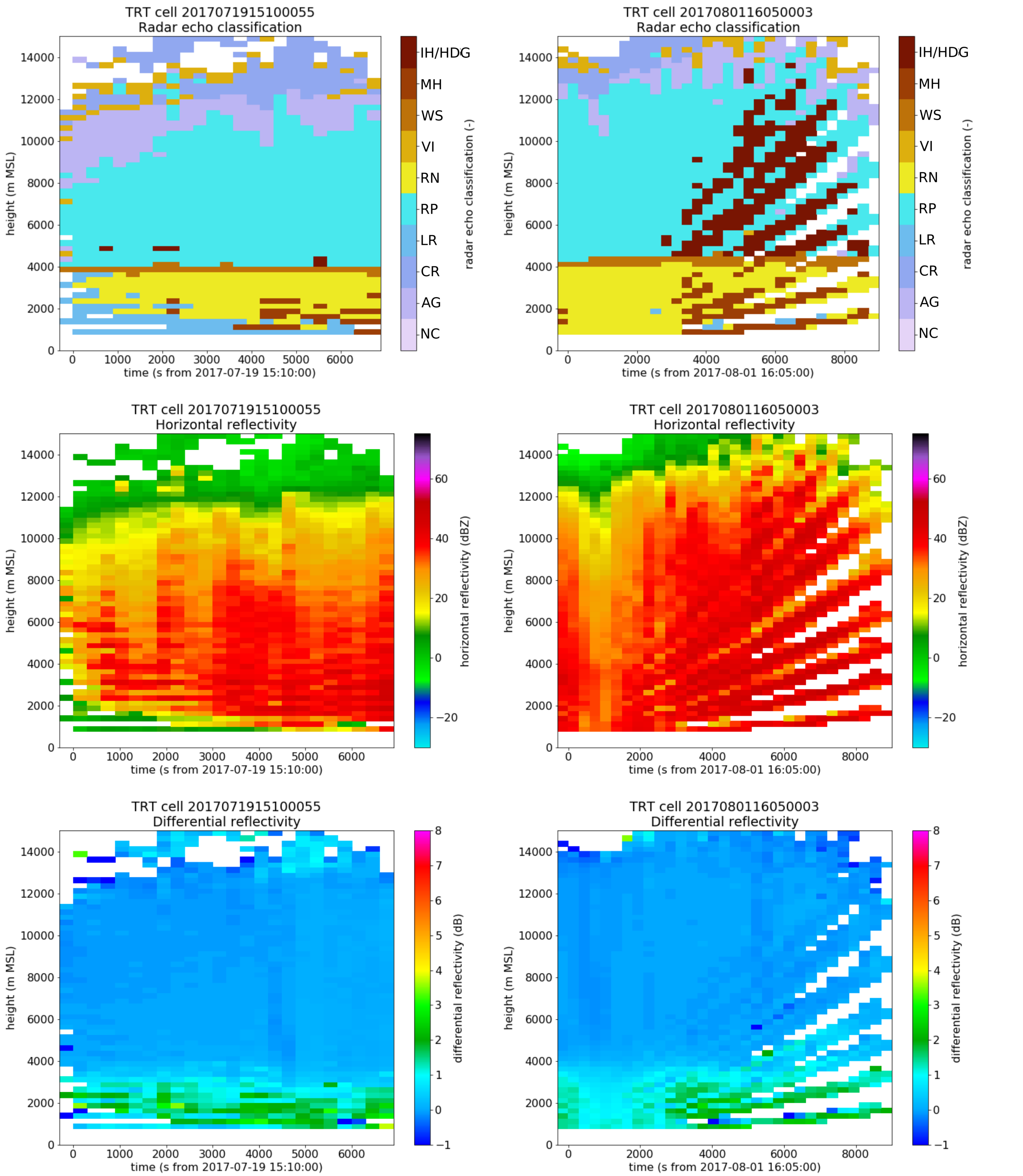


**Figure 14.** From top to bottom: Profile of hydrometeor class (mode at each level), profile of reflectivity (median values at each height level), profile of $Z_{dr}$. Left: Cell 1, Right: Cell 2

Atmos. Meas. Tech. Discuss., https://doi.org/10.5194/amt-2019-135
Manuscript under review for journal Atmos. Meas. Tech.
Discussion started: 23 April 2019


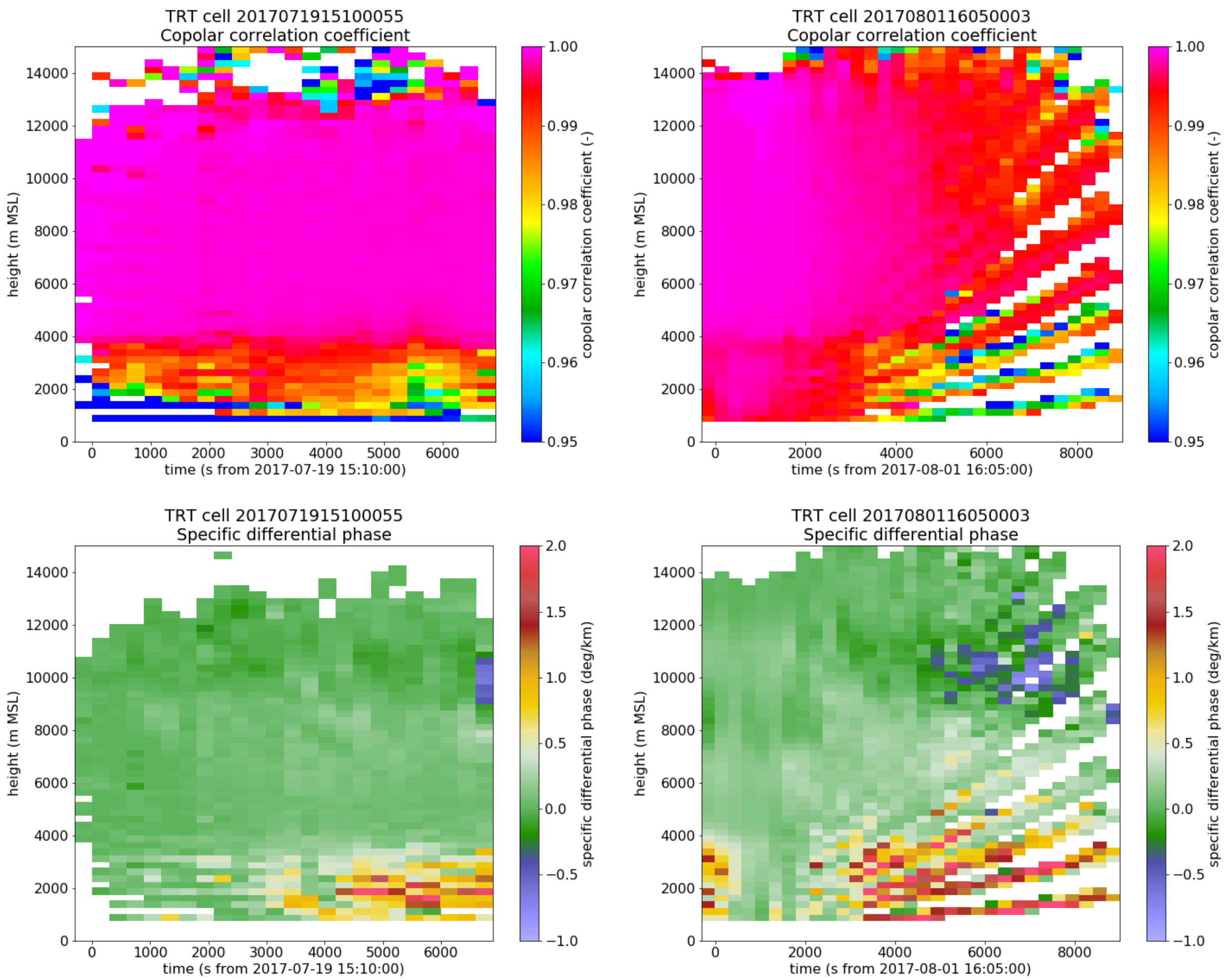


**Figure 15.** Top: Profile of $\rho_{hv}$, Bottom: Profile of $K_{dp}$. Left: Cell 1, Right: Cell 2

Atmos. Meas. Tech. Discuss., https://doi.org/10.5194/amt-2019-135
Manuscript under review for journal Atmos. Meas. Tech.
Discussion started: 23 April 2019


Atmospheric Measurement Techniques
Discussions

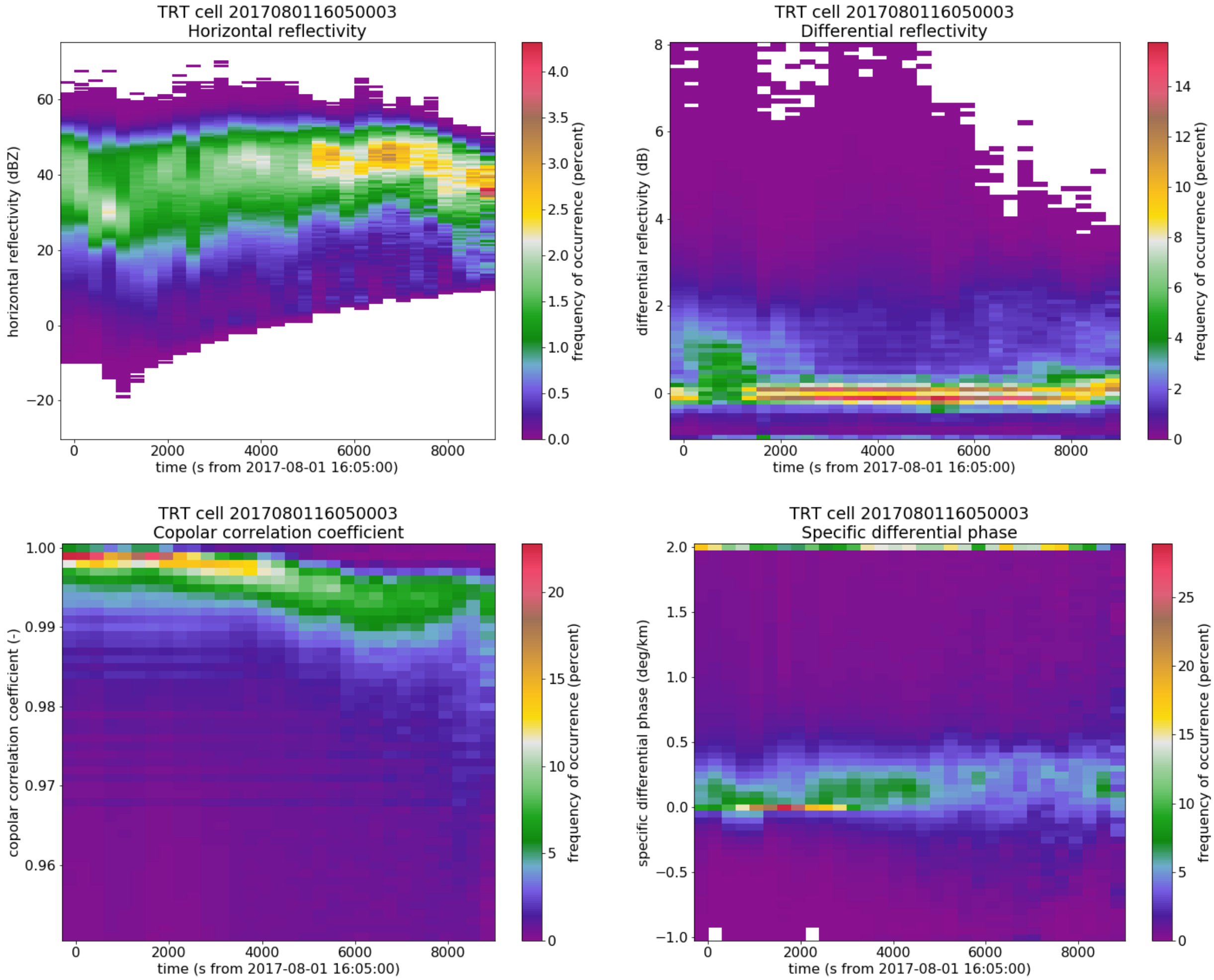


**Figure 16.** Percentage of occurrence at each time step of from top to bottom and left to right: Reflectivity, $Z_{dr}$, $\rho_{hv}$ and $K_{dp}$ for cell 2